

# Effect of growth time on the optical constants of ZnO nanowires by hydrothermal synthesis for application in optoelectronic devices

E. MUCHUWENI<sup>1,2,\*</sup>, T. S. SATHIARAJ<sup>1</sup>, H. NYAKOTYO<sup>1,2</sup>, C. SHONHIWA<sup>2</sup>, M. T. MAGAMA<sup>2</sup>

<sup>1</sup>Department of Physics and Astronomy, Botswana International University of Science and Technology (BIUST), P. Bag 16, Palapye, Botswana

<sup>2</sup>Department of Physics and Engineering, Bindura University of Science Education (BUSE), P. Bag 1020, Bindura, Zimbabwe

Recently, an assortment of zinc oxide (ZnO) nanostructures, such as nanowires, nanorods, nanobelts, nanoribbons and nanoflowers, have attracted significant research attention in the fabrication of optoelectronic devices, especially as transparent conductive electrodes and electron transport layers (ETLs) due to their high optical transmittance in the visible region and excellent electrical conductivity. Among these nanostructures, ZnO nanowires have been prepared using hydrothermal synthesis, and their optical constants, such as refractive index ( $n$ ) and extinction coefficient ( $k$ ), were determined as a function of growth time. In the visible region,  $n$  and  $k$  showed an increasing trend with growth time, which was associated with the decrease in optical transmittance owing to the growth of longer nanowires with relatively high reflectance and high absorbance. Despite the decrease in transmittance with increasing growth time, there was an increase in electron concentration ( $N_c$ ), favourable for transparent electrode and ETL applications. This was ascribed to an increase in the mean crystallite sizes, which produces less grain boundaries; hence, few charge carrier traps and scattering centres. The effect of growth time on the optical band gap ( $E_g$ ), Urbach energy ( $E_u$ ), effective single oscillator energy ( $E_o$ ), dispersion energy ( $E_d$ ), zero frequency dielectric constant ( $\epsilon_0$ ), zero frequency refractive index ( $n_0$ ) and high frequency dielectric constant ( $\epsilon_\infty$ ) was also investigated. Raman spectroscopy also revealed the presence of  $E_2$  (high) and  $A_1$  (LO) modes, whose intensity increased with growth time, demonstrating an improvement in crystallinity and an increase in structural defects, such as oxygen vacancies, which act as donors that increase  $N_c$ , in consistency with optical and electrical measurements. Thus, optical constants conceivably provide more insight into the optoelectronic properties of materials, and tuning of the hydrothermal parameters, e.g., growth time, plays a significant role in tailoring the optoelectronic performance of devices.

(Received January 23, 2021; accepted August 10, 2022)

**Keywords:** ZnO nanowires, Optical constants, Hydrothermal growth time, Raman spectroscopy, Optoelectronic devices

## 1. Introduction

Zinc oxide (ZnO) nanostructures, such as nanorods, nanowires, nanobelts, nanoflowers, nanoribbons and nanotubes, have received considerable research attention in recent years due to their novel optoelectronic properties and diverse applications, which substantially deviate from those of their bulk and thin film counterparts [1-5]. Among these nanostructures, ZnO nanowires are more appealing for application in optoelectronic devices, especially as transparent conductive electrodes and electron transport layers (ETLs) due to their high optical transmittance in the visible region and excellent electrical conductivity [6-8]. ZnO nanowires are commonly grown using the hydrothermal method, which has merits of low-cost, simple experimental setup, low growth temperature, low power consumption, substrate flexibility and large-scale production [9, 10].

The optical properties of ZnO nanowires grown by hydrothermal synthesis have been reported in a previous work [11]. However, the previous study did not go as far as investigating the optical constants, which if determined

provide crucial information regarding the optoelectronic properties of materials. Therefore, this work expands the previous study by investigating the effect of hydrothermal growth time on the optical parameters of ZnO nanowires, including the refractive index ( $n$ ), extinction coefficient ( $k$ ), optical band gap ( $E_g$ ), Urbach energy ( $E_u$ ), effective single oscillator energy ( $E_o$ ), dispersion energy ( $E_d$ ), zero frequency dielectric constant ( $\epsilon_0$ ), zero frequency refractive index ( $n_0$ ), high frequency dielectric constant ( $\epsilon_\infty$ ) and free electron concentration ( $N_c$ ). Raman spectroscopy was also performed to give more insight into the vibrational modes of the ZnO nanowires. Knowledge of these optical and vibrational properties plays a key role in the design and fabrication of high performance next-generation optoelectronic devices.

## 2. Experimental details

ZnO nanowires were prepared by hydrothermal synthesis at various growth times (2 - 8 h), as reported elsewhere [11]. Their Raman spectra were obtained using

a Horiba–Jobin Yvon Raman spectrometer (LabRAM HR Evolution, France), in the wavenumber range  $70\text{--}700\text{ cm}^{-1}$ . Their optical transmittance spectra were obtained in the  $300\text{--}800\text{ nm}$  wavelength range using the UV/Vis/NIR spectrophotometer (Lambda-750, Perkin-Elmer, USA). The transmittance data was used to determine  $n$  and  $k$  through optical modelling using the Optichar software, version 11.65. The values of  $n$  and  $k$  were then used to determine crucial optical parameters, such as  $E_g$ ,  $E_u$ ,  $E_o$ ,  $E_d$ ,  $\varepsilon_0$ ,  $n_0$ ,  $\varepsilon_\infty$  and  $N_c$ .

Since this work is an expansion of a previous study, the other characterizations by X-ray diffraction (XRD), field-emission scanning electron microscopy (FE-SEM), spectrophotometry and four-point probe resistivity measurements, can be found in ref. [11].

### 3. Results and discussion

Fig. 1 shows the Raman spectra of ZnO nanowires prepared at various growth times. All samples exhibited ZnO  $E_2$  (low),  $E_2$  (high) and  $A_1$  (LO) vibration modes, which were closer to the stress-free ZnO wavenumber values of  $102$ ,  $439$  and  $574\text{ cm}^{-1}$  [12]. Interestingly, the intensity of the  $E_2$  (high) mode increased with growth time, which indicated an improvement in crystallinity, in good agreement with XRD results [11]. The intensity of the  $A_1$  (LO) mode also increased with growth time, indicating an increase in structural defects, such as oxygen vacancies, which act as donors that increase  $N_c$ . This was consistent with electrical measurements reported elsewhere [11]. The other peaks at  $275$ ,  $330$  and  $510\text{ cm}^{-1}$  were associated with the  $B_1$  (high)– $B_1$  (low) multi-phonon mode [13], second order Raman processes [12], and Si in the glass substrate [12–14], respectively.

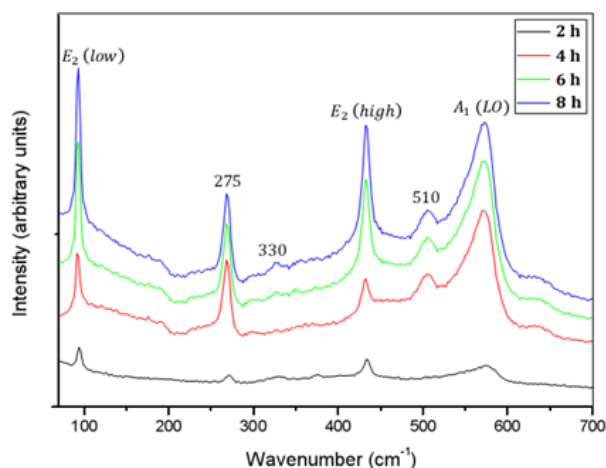


Fig. 1. Raman spectra of ZnO nanowires grown at 2–8 h (colour online)

The FE-SEM micrograph of ZnO grown at 8 h and the optical transmittance spectra of ZnO nanowires grown at 2–8 h, are shown in Figs. 2 and 3, respectively, as presented and discussed elsewhere [11].

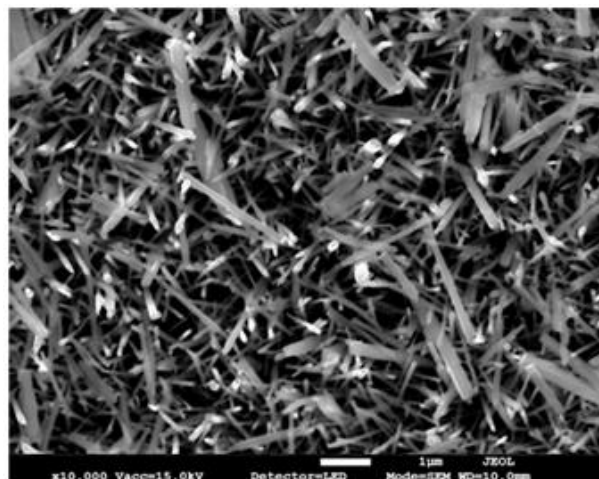


Fig. 2. FE-SEM micrograph of ZnO grown at 8 h

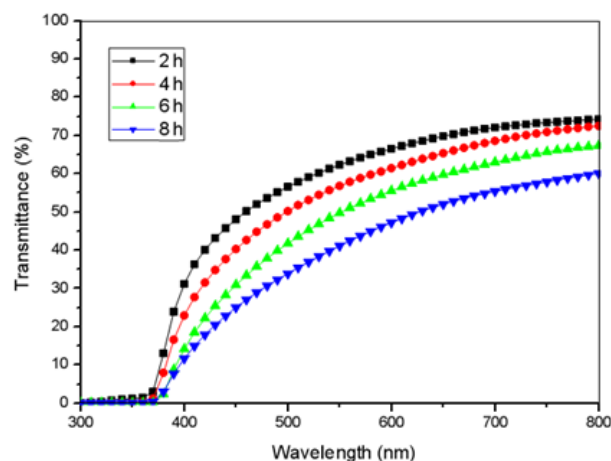


Fig. 3. The optical transmittance spectra of ZnO nanowires grown at 2–8 h (colour online)

The optical transmittance data was used to determine  $n$  and  $k$  through optical modelling. In the visible region,  $n$  had nearly constant values, between  $\sim 1.6$  and  $2.3$ , as shown in Fig. 4, when compared with  $\sim 1.6\text{--}2.0$  for the gallium and aluminium co-doped ZnO (GAZO) thin films, used as seed layers for nanowire growth [15]. This demonstrated that the ZnO nanowires had a relatively higher reflectance in the visible region, which made them to be less transparent, and hence more attractive for use in light scattering devices. Also, the refractive index increased with growth time in the visible region, which was attributed to the observed decrease in transmittance due to the increase in surface roughness, emanating from the growth of relatively long nanowires, which blocked the passage of more light at longer growth time, as revealed by the FE-SEM micrograph and transmittance spectra in Figs. 2 and 3, respectively.

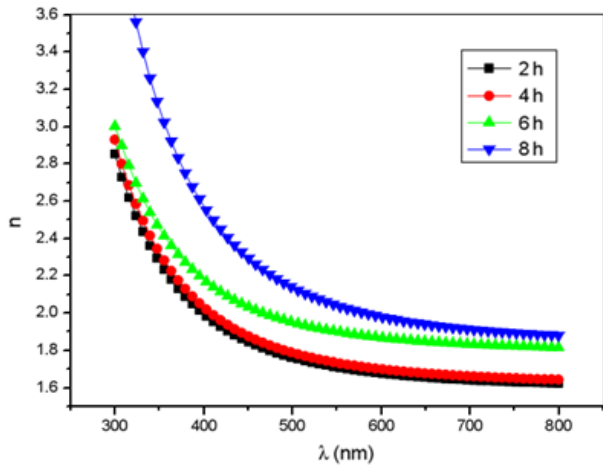


Fig. 4. The refractive index of ZnO nanowires as a function of growth time (colour online)

The spectral dependence of  $k$  with growth time was plotted in Fig. 5, and it displayed very low  $k$  values between  $\sim 0.05$  and  $0.20$  in the visible region, which were attributed to the high transparency nature of the nanowire samples. However, these  $k$  values were slightly greater than those for the GAZO thin film seed layers [15], demonstrating that the ZnO nanowires were relatively more absorbing to visible light than the GAZO thin films. This makes ZnO nanowires more appealing for use in photon energy harvesting applications, when compared with their thin film counterparts.

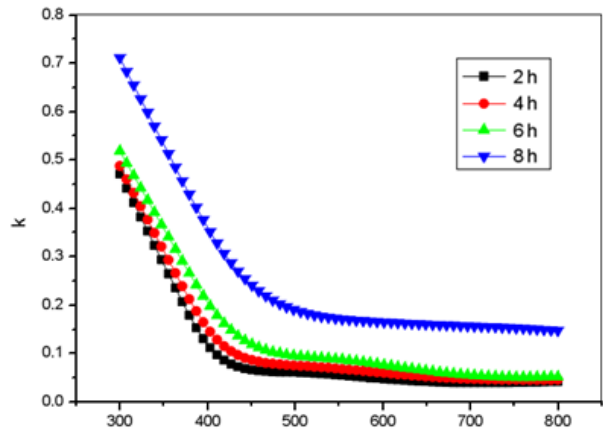


Fig. 5. The extinction coefficient of ZnO nanowires grown at various durations (colour online)

The extinction coefficient was used to determine the optical absorption coefficient ( $\alpha$ ) using Equation (1) [16]:

$$\alpha = \frac{4\pi k}{\lambda} \quad (1)$$

where  $\lambda$  is the wavelength of the incident photons. The absorption coefficient was then used to estimate the optical band gap,  $E_g$  (Tauc), by assuming a direct exciton transition between the valence and conduction bands, using the Tauc plot, shown in Fig. 6. The optical band gap was determined

by extrapolating the linear portion of the graph of  $(ah\nu)^2$  versus  $h\nu$ , to intercept the  $h\nu$  axis, where  $h\nu$  is the incident photon energy, and the obtained values were recorded in Table 1.  $E_g$  (Tauc) showed a decreasing trend with increasing growth time, which was attributed to the increase in structural defects and disorder represented by  $E_u$  [17, 18].

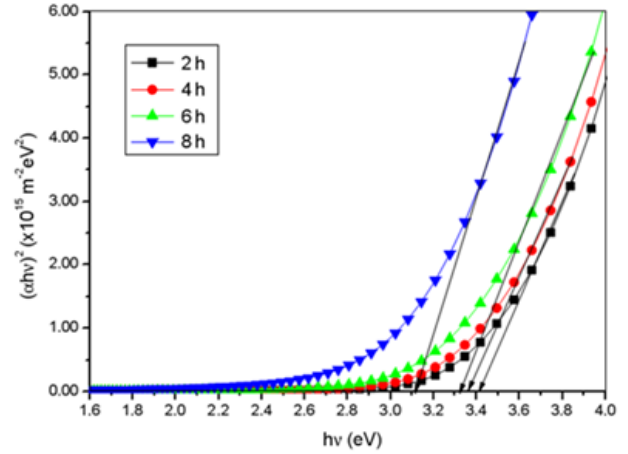


Fig. 6. Variation of  $(ah\nu)^2$  versus  $h\nu$  with growth time (colour online)

Table 1. The variation of  $E_g$  (Tauc),  $E_g$  (WDD),  $E_u$ ,  $E_o$ ,  $E_d$ ,  $\epsilon_0$ ,  $n_0$ ,  $\epsilon_\infty$ ,  $N_c/m^*$  and  $N_c$  with growth time

Optical properties	Growth time (h)			
	2	4	6	8
$E_g$ (Tauc) (eV)	3.41	3.36	3.32	3.12
$E_g$ (WDD) (eV)	3.27	3.16	3.14	3.11
$E_u$ (meV)	404	480	594	796
$E_o$ (eV)	6.53	6.32	6.29	6.23
$E_d$ (eV)	9.99	10.05	13.73	14.40
$\epsilon_0$	2.53	2.59	3.18	3.31
$n_0$	1.59	1.61	1.78	1.82
$\epsilon_\infty$	3.25	3.35	3.97	4.89
$N_c/m^*$ ( $\times 10^{27}$ kg $^{-1}$ m $^{-3}$ )	1.46	1.55	1.59	3.22
$N_c$ ( $\times 10^{20}$ cm $^{-3}$ )	3.20	3.39	3.48	7.04

$E_u$  was determined from the reciprocal of the gradient of the linear fit of  $\ln \alpha$  versus  $h\nu$ , shown in Fig. 7, and the obtained values were recorded in Table 1.  $E_u$  increased with growth time, which indicated an increase in the density of all possible defects and disorders, incurred during nanowire growth, such as lattice defects and stress [18]. Hence, the high defect concentration and structural disorder at longer growth durations results in more light scattering centres, which eventually lower the optical transmittance [19], as revealed earlier in Fig. 3. This was consistent with Raman spectroscopy, discussed earlier, which revealed an increase in structural defects, such as oxygen vacancies, that serve as electron donors to increase  $N_c$ , and hence improve the optoelectronic performance of materials.

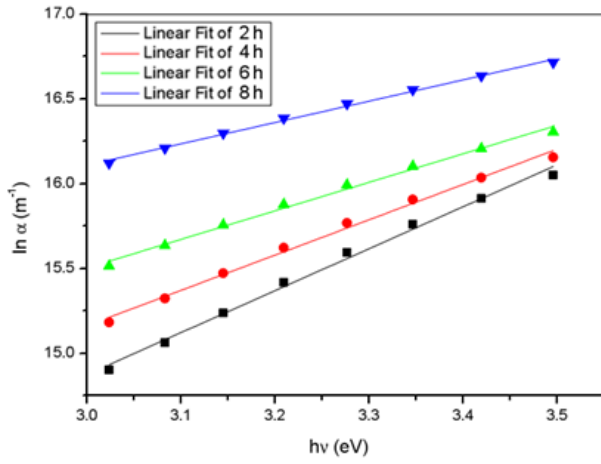


Fig. 7. A plot of  $\ln \alpha$  versus  $h\nu$  as a function of growth time (colour online)

The dependence of refractive index on photon energy was determined in the weak absorption region using the Wemple and DiDomenico (WDD) single oscillator dispersion model [20, 21], by plotting Fig. 8, which shows the variation of  $(n^2-1)^{-1}$  with  $(h\nu)^2$ . This was used to determine  $E_o$  and  $E_d$  from the slope  $(1/(E_o E_d))$  and intercept  $(E_o/E_d)$ , respectively. The obtained values were listed in Table 1 and were in good agreement with those reported by Orainy [22], Ahmmad et al. [23], Bedia et al. [24] and Yakuphanoglu et al. [25].  $E_o$  decreased with increasing growth time, which was associated with the increase in structural disorder and defects, as revealed earlier by Raman study and  $E_u$ . On the other hand,  $E_d$  increased with growth time, which was related to the improvement in microstructural order, as demonstrated elsewhere by FE-SEM [11].

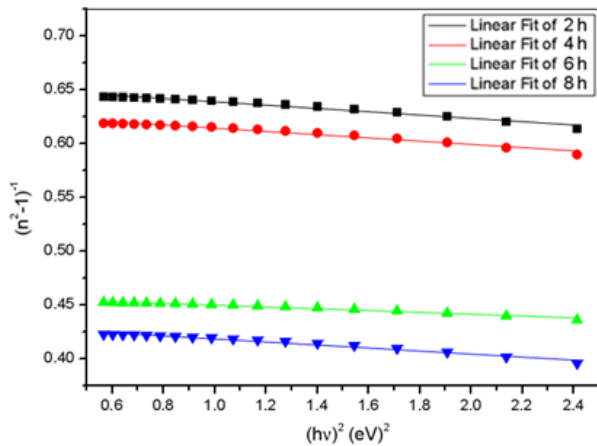


Fig. 8. A plot of  $(n^2-1)^{-1}$  with  $(h\nu)^2$  for the ZnO nanowires prepared at different growth times (colour online)

$E_o$  was used to estimate the optical band gap,  $E_g$  (WDD), using Equation (2) [26]:

$$E_g(WDD) \approx \frac{1}{2} E_o \quad (2)$$

The obtained values were recorded in Table 1. These were consistent with those obtained using the Tauc method and followed the same decreasing trend with increasing growth time.  $E_o$  and  $E_d$  were also used to determine  $\epsilon_0$  and  $n_o$  using Equations (3) and (4) [27]:

$$\epsilon_0 = 1 + \frac{E_d}{E_o} \quad (3)$$

$$n_o = \sqrt{\epsilon_0} \quad (4)$$

The obtained values were recorded in Table 1 and were consistent with previous studies [15, 25, 27-29].  $\epsilon_0$  and  $n_o$  showed an increasing trend with growth time, which was attributed to the decrease in visible optical transmittance at longer growth time.

In the weak absorption region, when  $n^2 \gg k^2$ ,  $n^2$  can be expressed using Equation (5) [23]:

$$n^2 = \epsilon_\infty - \left[ \frac{e^2}{4\pi^2 c^2 \epsilon_0} \right] \left[ \frac{N_c}{m^*} \right] \lambda^2 \quad (5)$$

where  $e$  is the electronic charge,  $m^* = 0.24 m_e$  [30] is the effective mass of the free electron,  $m_e$  is the free electron mass and  $c$  is the speed of light. The values of  $N_c/m^*$  and  $\epsilon_\infty$  were respectively determined from the slope and intercept of the plot of  $n^2$  versus  $\lambda^2$ , shown in Fig. 9, and the obtained values were recorded in Table 1, together with those of  $N_c$ .

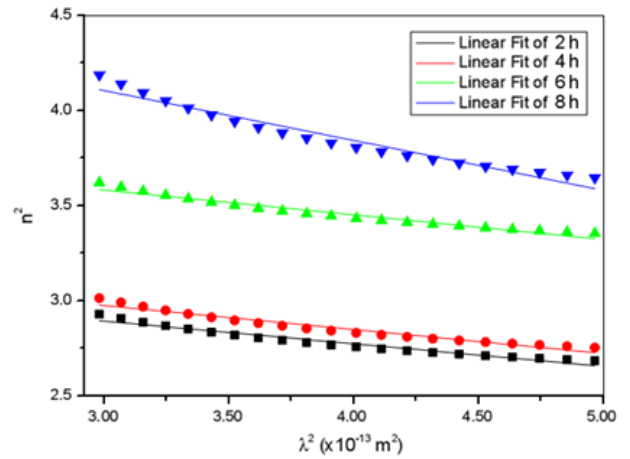


Fig. 9. A plot of  $n^2$  versus  $\lambda^2$  for the ZnO nanowires grown at various durations (colour online)

The values for the high frequency dielectric constant were closer to 3.75 for bulk ZnO [31].  $N_c/m^*$  and  $N_c$  increased with growth time, which implied an improvement in the electronic properties of the nanowires, in good agreement with our previous study [11]. This was also consistent with the increase in  $N_c$  revealed earlier by Raman study, and was attributed to the larger mean crystallite sizes, which produce few grain boundaries, and hence less charge carrier trapping and scattering centres at longer growth time.

#### 4. Conclusion

Optical constants of ZnO nanowires, such as  $n$  and  $k$ , were successfully determined and used to investigate other important optical parameters, such as  $E_g$ ,  $E_u$ ,  $E_o$ ,  $E_d$ ,  $\epsilon_0$ ,  $n_0$ ,  $\epsilon_\infty$  and  $N_c$ , as a function of hydrothermal growth time. Favourable optoelectronic properties were obtained at longer growth duration. Increasing the growth time led to an increase in structural defects, such as oxygen vacancies, which act as electron donors that increase the  $N_c$ ; hence, rendering the ZnO nanowires with ample potential for application in optoelectronic devices. This was consistent with electrical measurements and demonstrated the importance of tuning the hydrothermal growth time to optimize the properties of ZnO nanowires for optoelectronic applications.

#### Acknowledgements

This work was performed using Botswana International University of Science and Technology's research facilities.

#### References

- [1] U. Rehman, J. Jacob, A. Mahmood, K. Mahmood, A. Ali, A. Ashfaq, M. Basit, N. Amin, S. Ikram, S. Hussain, *J. Alloys Compd.* **843**, 156081 (2020).
- [2] W. Feng, C. Wu, X. Duan, *J. Optoelectron. Adv. M.* **22**(1-2), 81 (2020).
- [3] S. Jagadhesan, V. Senthilnathan, S. Senthil, *J. Optoelectron. Adv. M.* **20**(3-4), 188 (2018).
- [4] R. Bhardwaj, A. Bharti, J. P. Singh, K. H. Chae, N. Goyal, *Nanoscale Adv.* **2**, 4450 (2020).
- [5] B. G. Shohany, A. K. Zak, *Ceram. Int.* **46**, 5507 (2020).
- [6] S. Paul, J. Sultana, N. R. Saha, G. K. Dalapati, A. Karmakar, S. Chattopadhyay, *Optik* **228**, 166141 (2021).
- [7] E. Muchuweni, T. S. Sathiaraj, M. T. Magama, P. Dzomba, *J. Optoelectron. Adv. M.* **22**(3-4), 200 (2020).
- [8] I. L. P. Raj, S. Valanarasu, K. Hariprasad, J. S. Ponraj, N. Chidhambaram, V. Ganesh, H. E. Ali, Y. Khairy, *Opt. Mater.* **109**, 110396 (2020).
- [9] S. Yuvaraj, A. C. Fernandez, M. Sundararajan, C. S. Dash, P. Sakthivel, *Ceram. Int.* **46**, 391 (2020).
- [10] H. O. Chu, Q. Wang, Y.-J. Shi, S.-G. Song, W.-G. Liu, S. Zhou, D. Gibson, Y. Alajlani, *Trans. Nonferrous Met. Soc. China* **30**, 191 (2020).
- [11] E. Muchuweni, T.S. Sathiaraj, H. Nyakoty, *J. Alloys Compd.* **721**, 45 (2017).
- [12] K. A. Alim, V. A. Fonoberov, A. A. Balandin, *Appl. Phys. Lett.* **86**, 053103 (2005).
- [13] R. G. Waykar, A. S. Pawbake, R. R. Kulkarni, A. A. Jadhavar, A. M. Funde, V. S. Waman, H. M. Pathan, S.R. Jadhkar, *J. Mater. Sci. Mater. Electron.* **27**, 1134 (2016).
- [14] Q. Li, J. Bian, J. Sun, J. Wang, Y. Luo, K. Sun, D. Yu, *App. Surf. Sci.* **256**, 1698 (2010).
- [15] E. Muchuweni, T. S. Sathiaraj, J. Masanganise, N. Muchanyereyi, *J. Inorg. Organomet. Polym. Mater.* **29**, 48 (2019).
- [16] D. Y. Zhang, P. P. Wang, R. I. Murakami, X. P. Song, *Prog. Nat. Sci. Mater.* **21**, 40 (2011).
- [17] S. A. Ansari, M. M. Khan, S. Kalathil, A. Nisar, J. Lee, M. H. Cho, *Nanoscale* **5**, 9238 (2013).
- [18] M. H. Mamat, M. F. Malek, N. N. Hafizah, M. N. Asiah, A. B. Suriani, A. Mohamed, N. Nafarizal, M. K. Ahmad, M. Rusop, *Ceram. Int.* **42**, 4107 (2016).
- [19] X. L. Zhang, K. N. Hui, K. S. Hui, J. Singh, *Mater. Res. Bull.* **48**, 1093(2013).
- [20] S. H. Wemple, M. DiDomenico, *Phys. Rev. B* **3**, 1338 (1971).
- [21] S. H. Wemple, M. DiDomenico, *Phys. Rev. B* **1**, 193 (1970).
- [22] R. H. A. Orainy, *J. Sol-Gel Sci. Technol.* **70**, 47 (2014).
- [23] S. K. Ahmmad, M. A. Samee, A. Edukondalu, S. Rahman, *Results Phys.* **2**, 175 (2012).
- [24] A. Bedia, F. Z. Bedia, M. Aillerie, N. Maloufi, B. Benyoucef, *Energy Procedia* **50**, 603 (2014).
- [25] F. Yakuphanoglu, S. Ilican, M. Caglar, Y. Caglar, *J. Optoelectron. Adv. M.* **9**(7), 2180 (2007).
- [26] K. Tanaka, *Thin Solid Films* **66**, 271 (1980).
- [27] D. Komaraiah, E. Radha, Y. Vijayakumar, J. Sivakumar, M. V. R. Reddy, R. Sayanna, *Mod. Res. Catal.* **5**, 130 (2016).
- [28] G. Malik, J. Jaiswal, S. Mourya, R. Chandra, *J. Appl. Phys.* **122**, 143105 (2017).
- [29] E. R. Shaaban, M. E. Hagary, E. S. Moustafa, H. S. Hassan, Y. A. M. Ismail, M. E. Ismail, A. S. Ali, *Appl. Phys. A* **20**, 122 (2016).
- [30] S. J. Pearton, D. P. Norton, K. Ip, Y.W. Heo, T. Steiner, *Prog. Mater. Sci.* **50**, 293 (2005).
- [31] D. C. Look, *Mater. Sci. Eng. B.* **80**, 383 (2001).

\*Corresponding author: emuchuweni@buse.ac.zw